

See discussions, stats, and author profiles for this publication at: <https://www.researchgate.net/publication/265388273>

Semiconductor–halfmetal–metal transition and magnetism of bilayer graphene nanoribbons/hexagonal boron nitride heterostructure

ARTICLE *in* SOLID STATE COMMUNICATIONS · NOVEMBER 2014

Impact Factor: 1.9 · DOI: 10.1016/j.ssc.2014.08.008

CITATIONS

2

READS

53

5 AUTHORS, INCLUDING:



Victor Ilyasov

Don State Technical University

60 PUBLICATIONS 269 CITATIONS

[SEE PROFILE](#)



Chuong Nguyen

Don State Technical University

17 PUBLICATIONS 56 CITATIONS

[SEE PROFILE](#)



Semiconductor–halfmetal–metal transition and magnetism of bilayer graphene nanoribbons/hexagonal boron nitride heterostructure

V.V. Ilyasov ^{a,*}, B.C. Meshi ^a, V.C. Nguyen ^{a,*}, I.V. Ershov ^a, D.C. Nguyen ^b

^a Don State Technical University, Rostov on Don 344000, Russia

^b Hanoi University of Science and Technology, Hanoi 10000, Vietnam



ARTICLE INFO

Article history:

Received 2 April 2014

Received in revised form

27 May 2014

Accepted 12 August 2014

by Y.E. Lozovik

Available online 20 August 2014

Keywords:

A. Graphene nanoribbons

B. Electric field

C. Hexagonal boron nitride

E. Density functional theory

ABSTRACT

The paper presents the results of ab initio study of electronic structure modulation and edge magnetism in the antiferromagnetic (AF) bilayer zigzag graphene nanoribbons (AF-BZGNR)/hexagonal boron nitride (h-BN(0001)) semiconductor heterostructure induced with transverse external electric field (E_{ext}) and nanomechanical compression (extension), performed within the framework of the density functional theory using Grimme's DFT(PBE)-D2 scheme. For the first time we established critical values of E_{ext} and interlayer distance in the bilayer for the BZGNR/h-BN(0001) heterostructure providing for semiconductor–halfmetal–metal phase transition for one of the electron spin configurations. We discovered the effect of preserved local magnetic moment ($0.3\mu_B$) of edge carbon atoms of the lower (buffer) graphene nanoribbon during nanomechanical uniaxial compression (or extension) of the BZGNR/h-BN(0001) semiconductor heterostructure. It has been demonstrated that magnetic properties of the AF-BZGNR/h-BN(0001) semiconductor heterostructure can be controlled using E_{ext} . In particular, the local magnetic moment of edge carbon atoms decreases by 10% at a critical value of the positive potential. We have established that local magnetic moments and band gaps can be altered in a wide range using nanomechanical uniaxial compression and E_{ext} , thus making the AF-BZGNR/h-BN(0001) semiconductor heterostructure potentially promising for nanosensors, spin filters, and spintronics applications.

© 2014 Elsevier Ltd. All rights reserved.

1. Introduction

Bilayer zigzag graphene nanoribbons (BZGNRs), alongside with single-layer nanoribbons, represent an essential 1D carbon nanostructure for creation of electronic devices, sensors, solar cells and energy accumulation with their diverse and remarkable physical and chemical properties due to specific edge states and size effects [1–3]. In the ground state, the edge spin configuration of zigzag graphene nanoribbon (ZGNR) has antiferromagnetic (AF) ordering [4,5]. The ZGNR band structure with AF ordering (AF-ZGNR) corresponds to the semiconductor type [3,6–8]. Single-layer AF-ZGNR deposited on hexagonal boron nitride (h-BN(0001)) preserves edge ferromagnetism and semiconductor electronic structure [9,10]. At the same time, the energy gap in the AF-ZGNR/h-BN(0001) system increases with decrease of the nanoribbon width due to the quantum confinement effect and the substrate effect [1,5]. As a result of density functional theory (DFT) calculations [11], it has been established that application of E_{ext} across the width of ZGNR effectively cancels energy degeneracy of two edges thus making ZGNR spin-selective. In the presence

of a E_{ext} , AF-ZGNR may exhibit a semiconductor–halfmetal transition [1,8,13]. Bernal-stacked BZGNRs (AB) represent a zero-gap (gapless) semiconductor, in which the energy gap E_g may be induced by the interaction with the substrate [14,15], E_{ext} [1,16–20] and/or nanomechanical interlayer compression [1,21,22]. BZGNRs, just like single-layer ZGNRs, exhibit edge magnetism [23–25]. There are two possibilities for stacking of bZGNR: the so-called α and β stackings (AB_α and AB_β respectively) [26]. AB_α stacking is characterized by structural instability resulting in deformation of nanoribbon edges, in AB_β stacking there is no structural deformation so that nanoribbon layers are flat [23]. Therefore, further we shall only discuss the AB_β stacking. Four magnetic spin configurations of the edge states can be examined in the ab initio study of the BZGNR model [27]. Authors of [1,21,22] have demonstrated that electronic properties of spin-polarized AF-BZGNRs are very sensitive to the interlayer distance between ZGNRs. Addition of E_{ext} to uniaxial compression results in considerable rearrangement of the electron structure in AF-BZGNRs and, in particular, in the semiconductor–halfmetal transition for the spin down electron subsystem [1]. The above allows us to assume that the effects of E_{ext} , uniaxial compression (extension) and substrate interaction can be used to control and adjust the electronic and magnetic properties of functional devices. The said effects, combined with the effect of substrate-induced band gap opening, provide opportunities for creation of real graphene devices based on the

* Corresponding authors.

E-mail addresses: villy@mail.ru (V.V. Ilyasov), chuongnguyen11@gmail.com (V.C. Nguyen).

AF-BZGNR/h-BN(0001) heterostructure, for example, a field effect transistor (FET). Therefore, the potential opportunity for control of electronic properties introduces an intriguing aspect in the basic research of graphene materials.

Selection of the substrate type is essential for the modification of electronic and magnetic properties of BZGNRs. A study of modulation of magnetic and electronic properties induced by E_{ext} in the BZGNR/Si(001) system has demonstrated [16] that edge magnetism is only preserved in the upper nanoribbon layer. The lower BZGNR layer turns out to be non-magnetic and functions as a buffer layer tightly bound to the substrate. At the same time, BZGNRs without a substrate are known to exhibit edge magnetism in both nanoribbon layers [1]. Our DFT calculations have shown that BZGNRs on h-BN(0001) preserve edge magnetism in both graphene sheets and a small 0.38 eV gap opens in the zero-gap low-energy spectrum of graphene π -electrons [28].

The above allows us to suppose that the effects induced by a E_{ext} , uniaxial compression, and substrate and controlling the energy gap width and edge magnetism in such semiconductor structures as AF-BZGNR/h-BN(0001) are insufficiently studied so far. Therefore, in this paper we used the DFT calculations to examine the potential for modulation of spin-polarized electron structure and magnetic properties of the AF-BZGNR/h-BN(0001) semiconductor heterostructure with E_{ext} , nanomechanical interlayer compression (extension) and interaction with the substrate.

2. Model and method

The graphene heterostructure consists of the BZGNR placed on a h-BN(0001) substrate. BZGNR was the basic cell of the atomic structure used in the calculations. The ZGNR is located in the x - y plane. ZGNR width is made up by eight dimers of C atoms along the x -axis. Dangling bonds of the edge atoms were passivated with H atoms. The h-BN is characterized by weak interaction between the layers, interchange of B and N atoms from one layer to another in the [0001] direction and their location above each other. C atoms in the first graphene sublattice are located immediately above atoms on the surface, while atoms in the second sublattice are projected over the center of B-N lattice hexagons of the substrate surface.

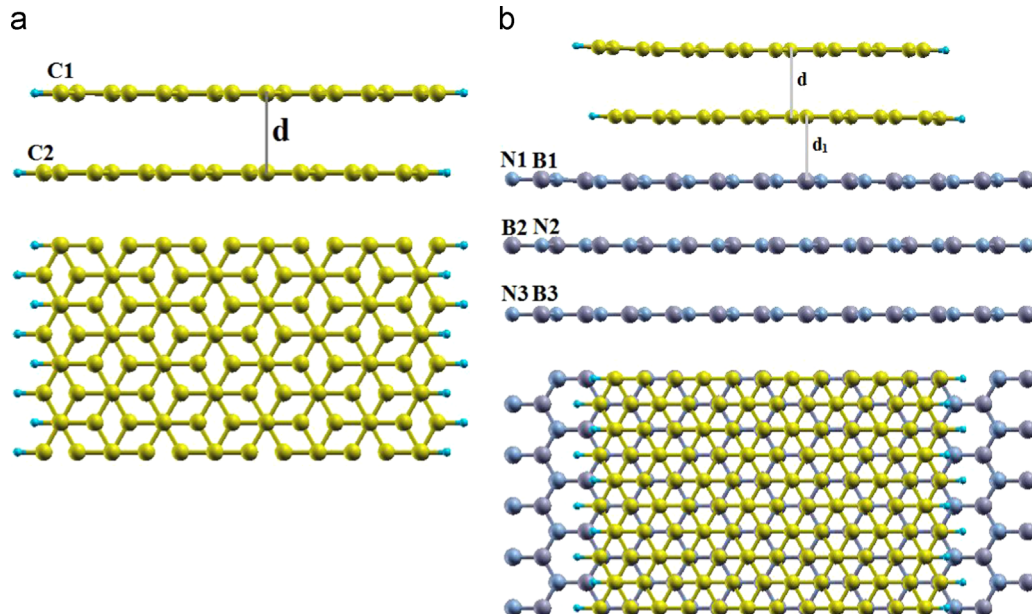


Fig. 1. The relaxed atomic structure of BZGNR (a) and BZGNR/h-BN(0001) (b) using DFT-D2 method where top – front view; bottom – top view.

To simulate a system consisting of substrate and BZGNR, we used a supercell containing unit cells of (4×4) h-BN and (4×4) graphene arranged within a plane (0001). The supercell parameter was selected to be divisible by the equilibrium value of the graphene unit cell parameter. Graphene cells were used to build an ZGNR. Fig. 1b demonstrates a fragment of the BZGNR/h-BN (0001) slab. The surface and the BZGNR/h-BN border were simulated as a slab consisting of three atomic layers of h-BN and a monolayer of ZGNR positioned at the distance of the d bond. Basic supercell consisted of 108 atoms. To prevent artificial intergraphene interactions, BZGNRs are separated by a sufficiently large vacuum space, edge-to-edge distance along the y direction and layer-to-layer distance along the z direction which are taken to be 10 Å and 25 Å, respectively.

In this paper, atomic and band structure calculations were performed using the Quantum Espresso (QE) software suite [29] based on the DFT [30–32] with spin polarization. Spin polarized calculation normally requires a fine sampling of the Brillouin zone, which we performed with a Monkhorst–Pack scheme of $30 \times 1 \times 1$ k -points. Plane wave and pseudopotentials were used as the calculations basic. Influence of the core electrons was accounted for by using ultrasoft pseudopotentials. Nonlocal exchange correlation functional was used in the Perdew–Burke–Ernzerhof (PBE, PBEsol) parametrization [33]. The plane waves cutoff energy for self-consistent field (SCF) calculation was 410 eV. Accomplished total cell energy convergence was at least 10^{-4} Ry/cell.

In the paper, we took into account the van der Waals interaction in our system within the DFT framework using a semiempirical potential introduced in the total energy functional (DFT-D2) in accordance with [34]: $E_{DFT-D2} = E_{DFT} + E_{disp}$. In DFT-D2 calculations we used well-known PBE exchange correlation functional with dispersion correction (PBE-D2).

Interaction of electrons with external electrostatic field along the y -axis is determined by the following expression similar to [35]:

$$U_{ext}(r) = |e| E \cdot r$$

U designation is used to distinguish the potential energy in electrostatic field from all other potential terms of the Kohn–Sham equation:

$$V_{KS}(r) = \int dr' \frac{n(r')}{|r - r'|} + V_{ion}(r) + V_{xc}(r)$$

Then Kohn-Sham equations can be interpreted considering the E_{ext} as

$$\left(-\frac{\hbar^2}{2m} \nabla^2 + V_{KS} + U_{ext} \right) \psi_i(r) = \epsilon_i \psi_i(r)$$

Applied electrostatic potential changes linearly along the entire unit cell; therefore, to observe the periodic boundary conditions, it has to be compensated to restore the original value at the cell border. For these purposes, the sawtooth potential shape with period equal to the unit cell period along the y -axis is most suitable (Fig. 2a). The scheme of relative placement of the slab and external electrostatic potential is shown in Fig. 2c. Hence it follows that if E_{ext} exists in the interval from 0 to l , while the simulated cell size is L along the y -axis, the gauge field E^* is defined as $E^* = -E_{ext}(l/L)$.

The “-” sign indicates that E^* direction is always opposite to the E_{ext} direction.

3. Results and discussion

3.1. Atomic and band structures of AF-BZGNR/h-BN(0001) heterostructure. Uniaxial compression (extension) effect

All four magnetic spin configurations of the edge states have been examined in the ab initio study of the BZGNR model as shown in Fig. 3a.

DFT calculations of total energy for these magnetic configurations have shown that the structure of BZGNRs with AF-FM edge

magnetic configuration (Fig. 3c) is the most stable one. Further we shall only discuss the AF-FM magnetic configuration in the BZGNRs. To study the atomic structure of the AF-BZGNR/h-BN (0001) interface, relaxation of two layers of ZGNR and one upper h-BN atomic plane of the slab was performed. Two lower layers of the h-BN(0001) substrate were “frozen”. Relaxation was carried out until the sum total of all forces in the system was reduced below 0.0001 eV/Å. We established equilibrium parameter values for the lattices, atomic positions of the nanoribbon and the upper layer of h-BN(0001), and the bond length ($d=0.339$ nm) between the ZGNR and substrate atomic layers. The distance between graphene layers in the nanoribbon reached $d=0.327$ nm, which is lower than that in crystalline graphite (0.335 nm). Obtained here results correlate well with known data [1,16]. DFT calculation results also demonstrated that the σ -bond lengths of planar h-BN (0001) can be described well using the PBE-D2 functional. In the AF-BZGNR/h-BN(0001) heterostructure, the C-C bond length for internal atoms of the nanoribbon reached 1.4290 Å. The bond length between two edge carbon atoms is 1.4070 Å indicating its deformation. This deformation is known to cause sharp peaks corresponding to the electron density states in the proximity of the Fermi level and induced local magnetic moment at the BZGNR edges.

In this part of the paper we used DFT calculations to study the responses of the band structure and edge magnetism to the effect of uniaxial interlayer compression (extension) in two cases: AF-BZGNR without substrate and the same on h-BN. For the highlighted AF-BZGNR/h-BN(0001) heterostructure fragment shown in

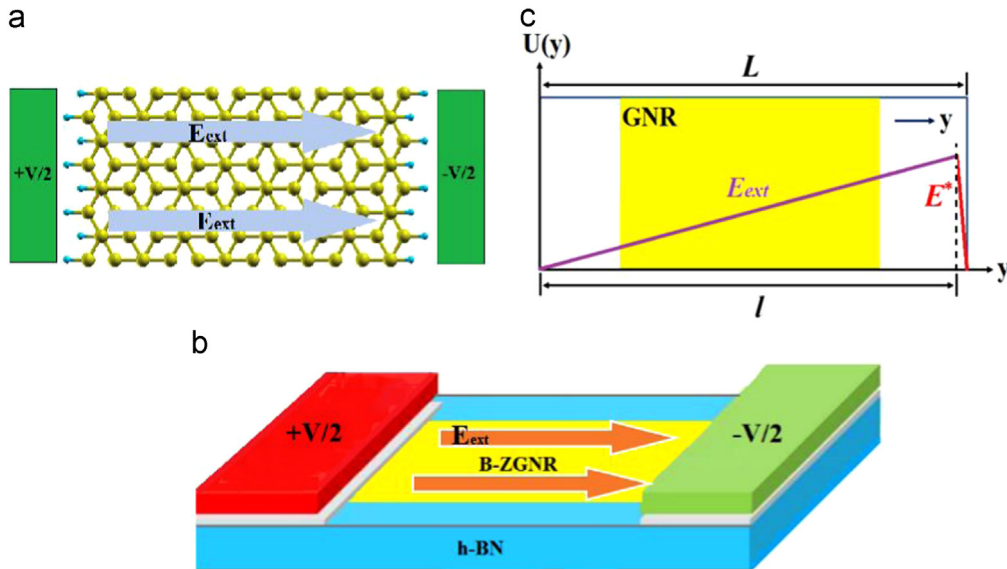


Fig. 2. (Color online) Schematic representation of the systems considered. (a) Diagram of the BZGNR with E_{ext} . E_{ext} has been applied along the cross-ribbon width, which is the y -axis direction. (b) Schematic of BZGNR deposited on h-BN substrate with E_{ext} along the y -axis direction (top). (c) Schematics of how to arrange saw-tooth potentials. The shaded yellow area represents the system under investigation and the empty white space is the vacuum. The purple and red solid lines denote the linear external electric potential and its counterpart. L is the size of the periodic cell along the y direction.

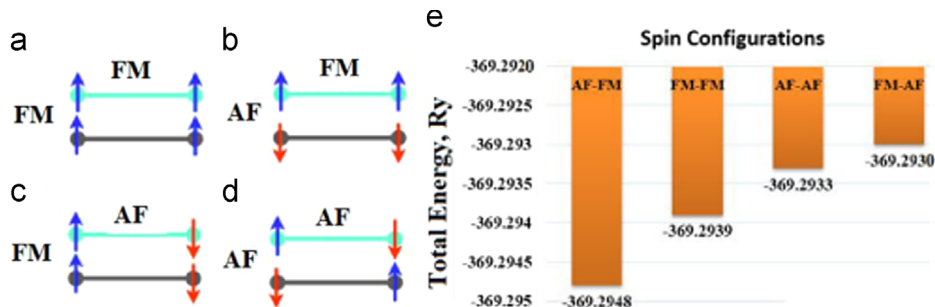


Fig. 3. Edge spin orientations in BZGNRs (a-d) and total energy of magnetic configurations (e).

Fig. 1b, we obtained in DFT calculations the total energy values (E_{tot}) as a function of interlayer distance in BZGNR (**Fig. 4a**). As follows from the analysis of **Fig. 4a**, the equilibrium state of the AF-BZGNR/h-BN (0001) system corresponds to the minimum total energy at the interlayer distance $d=0.327$ nm. Uniaxial compression or extension of the system makes its state metastable. The changes in the band structure and partial density of state (PDOS) in suspended AF-BZGNR in case of uniaxial compression (extension) are shown in **Fig. 5**.

Band structure of suspended relaxed AF-BZGNR with $d=0.327$ nm (**Fig. 5b**) corresponds to the semiconductor type characterized by the energy gap of $E_g=520$ meV in the low-energy spectrum of π -electrons. In case of nanomechanical bilayer compression to $d=0.237$ nm the low-energy spectrum of π -electrons undergoes considerable modification. The highest deformation of the bands is observed in the $k=\pi$ Dirac point, it is characterized by the energy gap $E_g=290$ meV. We have to add that the energy gap in the $k=2\pi/3$ Dirac point does not change and AF-BZGNR at $d=0.237$ nm remains a semiconductor. It should be noted that the fact is a new finding different from the results of [1], where a decrease of the interlayer distance to $d=0.24$ resulted in semiconductor–metal transition in

AF-ZGNR. In our view, this follows from the [L(S)DA] local density approximation used by the authors of [1] for the determination of the exchange correlation potential. However, local and semilocal approximations used for the description of the exchange and correlation energy (LDA, GGA, including PBEsol) within the DFT framework are known [12] to be incapable of a correct description of dispersion (van der Waals) interaction occurring in layered structures, including the system in question. We instead used the well-known PBE exchange correlation functional with dispersion correction (PBE-D2) [12]. In case of AF-BZGNR extension, i.e. an increase of the interlayer distance to $d=0.427$ nm, the low-energy spectrum of π -electrons changed insignificantly (**Fig. 5c**). We just have to note that at interlayer distance $d=0.427$ nm, a decrease in the energy splitting is observed in the bands belonging to the lower and upper bilayer ribbons. At the same time, interlayer compression considerably modifies the electronic properties of AF-BZGNR.

In the proximity of the Dirac points ($k=2\pi/3; k=\pi$), flat bands responsible for sharp peaks of PDOS are observed close to the Fermi level. PDOS of two edge carbon atoms C1 and C2 in AF-BZGNR are shown in **Fig. 5d–f** for the spin-up and spin-down electron

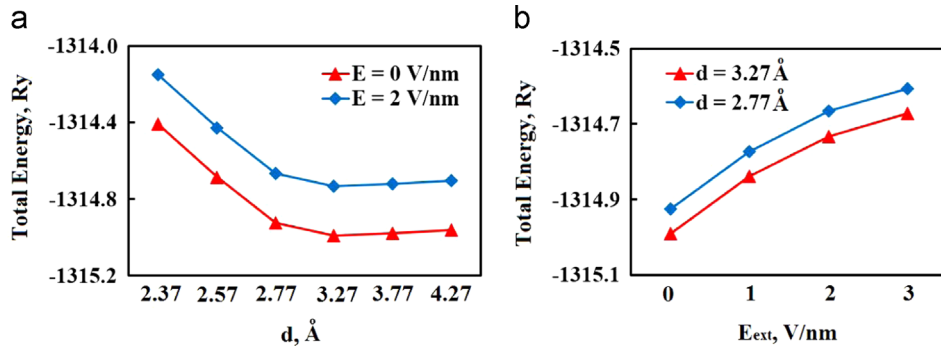


Fig. 4. DFT calculation of total energy for the AF-BZGNR/h-BN heterostructure depending on the (a) distance d (in Å) and (b) E_{ext} (V/nm).

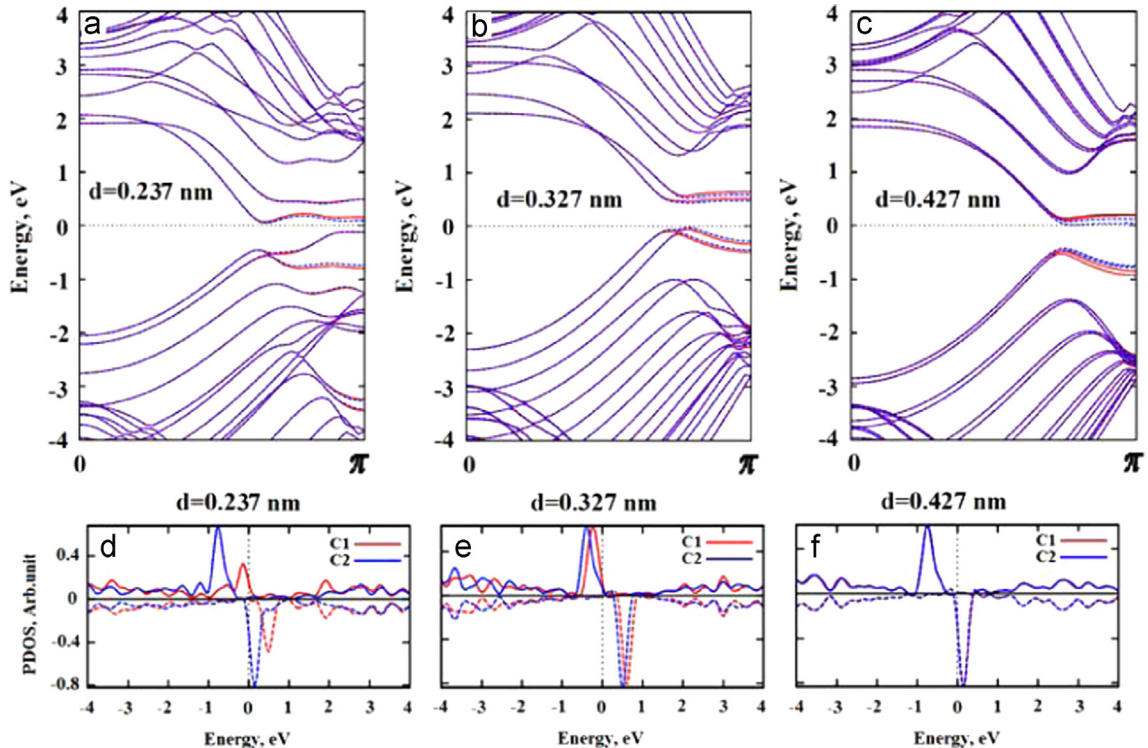


Fig. 5. (Color online) DFT-D2 calculations (a–c) of the band structure of the suspended AF-BZGNR for two spins (red – spin-up and blue – spin-down) and (d–f) PDOS of $2p_z$ -orbitals of carbon atoms (C1 – red and C2 – blue) in AF-BZGNR at varied interlayer distance for two spins: solid line – spin-up, dotted line – spin-down.

subsystems. Here only left edge carbon atoms are examined. Analysis of Fig. 5d-f shows that the largest redistribution of energy takes place in the edge states of the C1 electrons. For edge carbon atoms the size of PDOS peaks shift in the proximity of the Fermi level depends on the interlayer distance for the spin-up and spin-down electron configurations. In the absence of uniaxial compression the shift of localized edge states in the proximity of the Fermi level is 0.73 eV and 0.90 eV for C1 and C2 atoms respectively (Fig. 5e). With the distance decrease to 0.237 nm the noted shift decreases to 0.67 eV for the C1 edge carbon atom and remains constant for the C2 atom (Fig. 5d). An increase of the interlayer distance to 0.427 nm results in higher peaks' shift for the C1 atom and preserved shift size for the C2 atom (Fig. 5f). We should also note that at $d=0.427$ nm PDOS peaks of $2p_z$ -orbitals of carbon atoms (C1 and C2) are degenerate.

The changes in the band structure and PDOS in the AF-BZGNR heterostructure in case of uniaxial compression (extension) are shown in Figs. 6 and 7. Band spectrum of the relaxed AF-BZGNR/h-BN(0001) heterostructure with $d=0.327$ nm (Fig. 6d) corresponds to the semiconductor type characterized by energy gap in the $k=2\pi/3$ Dirac point. The gap size is 540 meV and 350 meV for the spin-up and the spin-down electron subsystem respectively. Therefore, compared with AF-BZGNR the band spectrum of the AF-8-BZGNR/h-BN(0001) heterostructure is noticeably modified due to the interaction with the substrate. Modification of the electron structure manifests itself as cancellation of energy

degeneracy for localized edge states of both spins and their splitting. In the $k=2\pi/3$ Dirac point the splitting energy reaches 190 meV. In case of nanomechanical graphene bilayer compression in the heterostructure to $d=(0.277; 0.257)$ the low-energy spectrum of π -electrons undergoes considerable modification, and band splitting increases (Fig. 6b and c). The AF-BZGNR/h-BN(0001) heterostructure at $d=0.277$ nm retains its semiconductor properties characterized by the 550 meV energy gap in the $k=2\pi/3$ Dirac point. There is no degeneracy in this point for the spin-up and spin-down electron subsystems. In the Brillouin zone segment between the $k=2\pi/3$ and $k=\pi$ points, band splitting is observed for both spins as well as considerable deformation of the occupied states band in the lower ZGNR. The energy gap in the $k=\pi$ Dirac point is 270 meV and 600 meV for the spin-up and spin-down electron subsystems. Electron structure of the AF-BZGNR/h-BN(0001) heterostructure compressed to the interlayer distance of $d=0.257$ nm can be interpreted as halfmetal or Mott semiconductor [36]. Finally, in the AF-BZGNR/h-BN(0001) heterostructure compressed to the interlayer distance $d=0.237$ nm the electron structure corresponds to the metal type (Fig. 6). The above indicates an opportunity for the semiconductor-halfmetal-metal transition resulting from uniaxial interlayer compression in the AF-BZGNR/h-BN(0001) system. With the opposite deformation direction, i.e. in case of interlayer extension of the AF-BZGNR/h-BN(0001) heterostructure to the interlayer distance $d=(0.377; 0.427)$ nm, the low-energy spectrum of π -electrons demonstrates

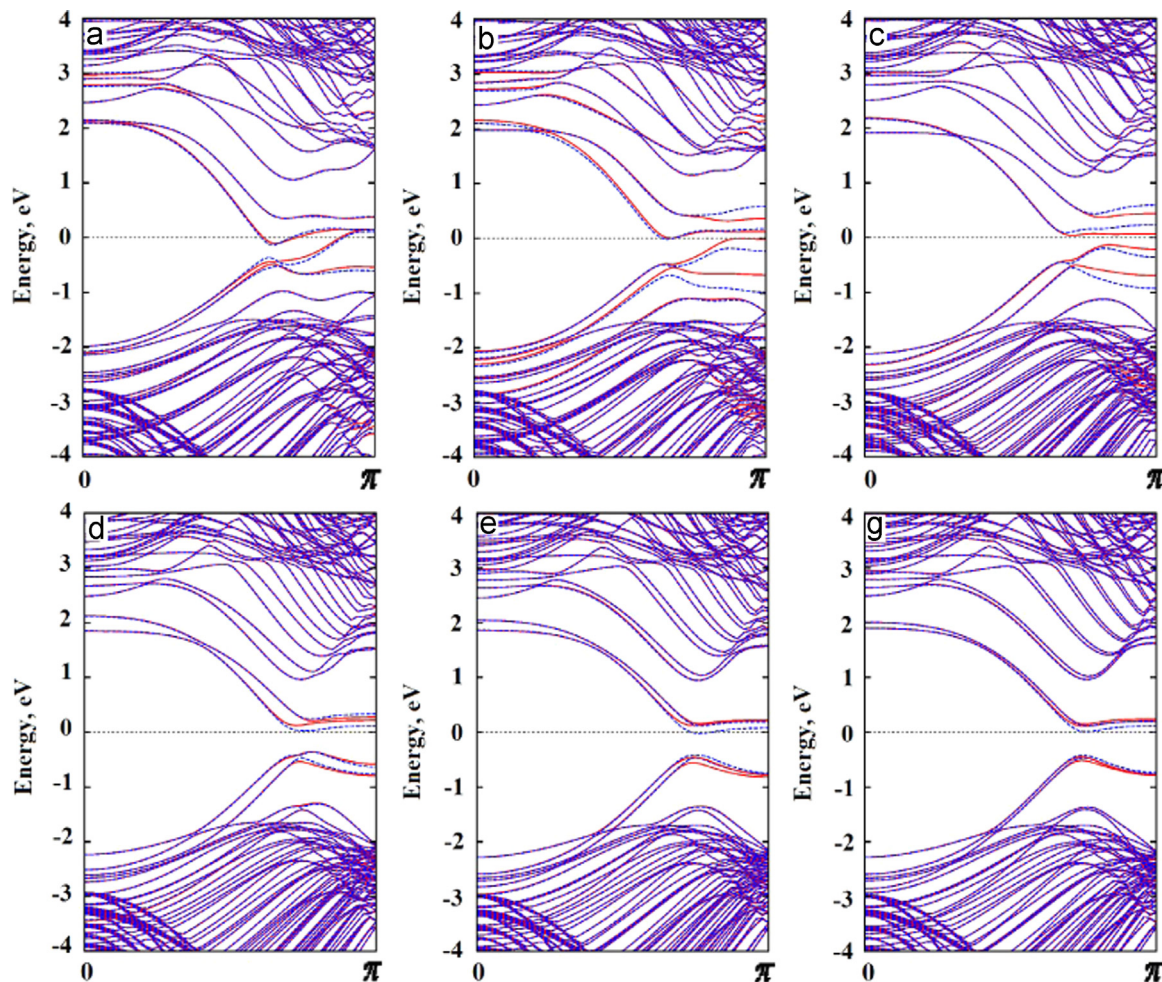


Fig. 6. (Color online) DFT-D2 calculation of the band structure in the AF-BZGNR/h-BN(0001) heterostructure for various interlayer distances d (nm): (a) 0.237 nm; (b) 0.257 nm; (c) 0.277 nm; (d) 0.327 nm; (e) 0.377 nm and (g) 0.427 nm for two spins: solid red line – spin-up, dotted blue line – spin-down.

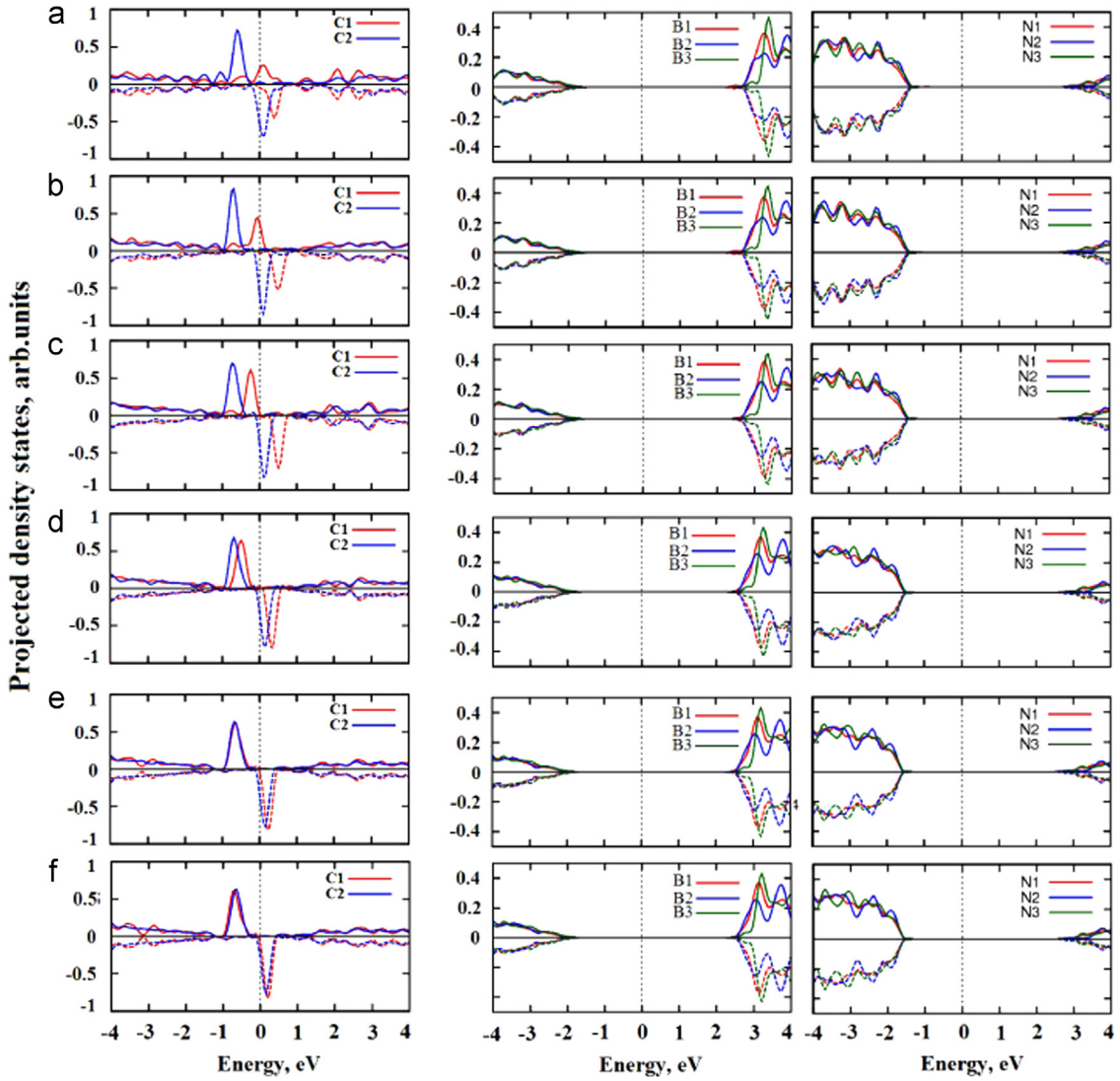


Fig. 7. (Color online) DFT-D2 calculation of PDOS for $2p_z$ -orbitals of carbon (C1 and C2), boron and nitrogen atoms in the AF-BZGNR/h-BN(0001) heterostructure at various interlayer distances d (nm): (a) 0.237 nm; (b) 0.257 nm; (c) 0.277 nm; (d) 0.327 nm; (e) 0.377 nm and (f) 0.427 nm for two spins: solid line – spin-up, dashed line – spin-down.

considerable lifting of band splitting and their partial degeneracy (Fig. 6e and g).

Thus, the result obtained after the study of band structure response in the AF-BZGNR/h-BN(0001) heterostructure to uniaxial interlayer compression and interaction with h-BN appears to be new. The study revealed the peculiarities of the modified band structure resulting from two effects: interlayer compression (extension) and interaction with the substrate. In particular, modification of the electron structure is also indicated by the position of the PDOS peaks of two edge carbon atoms (C1 and C2), boron atoms (B1, B2, and B3) and nitrogen atoms (N1, N2, and N3) in the AF-BZGNR/h-BN(0001) heterostructure shown in Fig. 7a–f for the spin-up and spin-down electron subsystems.

Analysis of Figs. 5 and 7 shows that in the AF-BZGNR/h-BN(0001) heterostructure, similar to suspended AF-BZGNR, the largest energy redistribution takes place in the edge states of the C1 atom electrons. However, the character of this transformation in the heterostructure is different. Common part for both systems is in the fact that for edge carbon atoms the size of sharp PDOS peaks shift in the proximity of the Fermi level depends on the interlayer distance for the spin-up and spin-down electron configurations, however, with addition of substrate effect. In the

absence of uniaxial compression, the shift of localized edge states in the proximity of the Fermi level is 0.39 eV and 0.46 eV for C1 and C2 atoms respectively (Fig. 7d), i.e. it is twice smaller compared with suspended AF-BZGNR. With the distance decreasing to 0.277 nm the noted shifts decrease to 0.27 eV and 0.33 eV for the C1 and C2 atoms respectively (Fig. 7c). We have to note additionally that PDOS peak for the spin-up electron subsystem of the C1 atom transforms into two peaks. The larger of them is at the Fermi level. Further interlayer compression of the AF-BZGNR/h-BN(0001) heterostructure to the distance of $d=0.257$ nm is characterized with the shift value for the C1 edge carbon atom decreased to 0.15 eV and the same remaining constant at 0.33 eV for the C2 atom (Fig. 5b). We should observe that during compression further modification of the energy structure occurs as well as a decrease in the statistical weight of the electron states making up the PDOS peaks in question. Finally, with the distance decrease to 0.237 nm the noted shifts increase to 0.39 eV and 0.46 eV for the C1 and C2 atoms respectively (Fig. 7a). The opposite deformation direction, i.e. increase of the interlayer distances to 0.377 nm and 0.427 nm respectively, does not alter the value of the PDOS peaks' shift for the C1 and C2 atoms (Fig. 7e and f) relatively to the equilibrium atomic structure of the AF-BZGNR/h-BN(0001) system. We should

note that at $d=0.427$ nm PDOS peaks of $2p_z$ -orbitals of carbon atoms (C1 and C2) are degenerate. It should be noted that the semiconductor–halfmetal–metal transition in the AF-BZGNR/h-BN(0001) heterostructure induced by the effects of uniaxial compression and substrate interaction is a distinctive feature in the modification of C1 edge states.

In this part of the paper we used DFT calculations to establish the dependence of the local magnetic moment value at the C1 and C2 edge carbon atoms in the AF-BZGNR/h-BN(0001) heterostructure upon the force of uniaxial interlayer compression (extension) and the substrate effect. Fig. 8 demonstrates local magnetic moments of the edge carbon atoms in BZGNR/h-BN(0001) depending on the compression (extension) value. As follows from the analysis of Fig. 8, local magnetic moments of the C1 atom depend on the interlayer compression, decreasing three times with the deformation of interlayer compression to $d=0.237$ nm. Local magnetic moments of the C2 atom in the lower ZGNR remain practically unchanged (Fig. 8). The reason of the noted difference between magnetic moments of the C1 and C2 atoms may be related to interlayer transition of some electrons from the spin-up subsystem of atoms C1 to C2, observed by the authors of [1]. The response of edge magnetism to the interlayer compression and interaction with the substrate may be caused by the modification of edge states in the C1 atom.

3.2. Band structures and magnetism of AF-BZGNR/h-BN(0001) heterostructure. Electric field effect

Early ab initio DFT calculations established [1] that E_{ext} applied across the width of suspended BZGNR induces in it the semiconductor–halfmetal transition at the critical E_{ext} value over 3 V/nm. Our DFT calculations have demonstrated that band spectrum in the AF-BZGNR/h-BN(0001) heterostructure, similar to the BZGNR system without substrate, exhibits dependence on the applied E_{ext} as shown in Fig. 9. DFT calculations of total energy for a heterostructure fragment (Fig. 1b) in this magnetic configuration have shown that in the examined interval of E_{ext} the total energy value increases insignificantly (0.02%), as illustrated in Fig. 4b. As we have noted above, in the absence of E_{ext} and uniaxial compression, band spectrum of the AF-BZGNR/h-BN(0001) heterostructure exhibits band gap $E_g=0.54$ eV and 0.35 eV for the spin-up and spin-down electron subsystems respectively. With the increase of the E_{ext} , the AF-BZGNR/h-BN(0001) heterostructure shows an increase of the energy gap for the spin-up electron subsystem. At the same time, for the spin-down electron subsystem we observe a decrease of the said gap and at a certain critical value of the E_{ext} closure of the band gap takes place. The effect is shown in

Fig. 9d demonstrating overlapping bands of edge carbon atoms for the spin-down electron subsystem.

It should be noted that the effect of E_{ext} essentially manifests itself as cancellation of energy degeneracy for localized edge states (both spins). An effect like that becomes possible because the energy of edge states shifts in the reverse directions for two spins [1]. Addition of the substrate effect to the E_{ext} effect results in an increase of the noted splitting evidently illustrated in Fig. 9b and f. Semimetallic character for the spin-down electron subsystem is accomplished in the AF-BZGNR/h-BN(0001) heterostructure when the critical E_{ext} value of 3 V/nm is applied (Fig. 9d). For suspended AF-BZGNR, semimetallic character is not achieved yet at values of the E_{ext} of 3 V/nm (Fig. 9h).

Thus, DFT calculations were used as the basis in order to establish critical values of E_{ext} for the AF-BZGNR/h-BN(0001) heterostructure providing for semiconductor–halfmetal transition for one of the spin electron configurations. Under critical value of the positive E_{ext} of 3 V/nm (Fig. 9d) the spin-down electron subsystem in the heterostructure undergoes the semiconductor–halfmetal transition, while for the spin-up electron subsystem we observe an increase of the band gap to 0.76 eV and 1.38 eV for the Dirac points $k=2\pi/3$ and $k=\pi$ respectively. Fig. 10a demonstrates the relation between the change character E_g and the value of E_{ext} force. Fig. 10b offers for comparison the effects of E_{ext} and uniaxial interlayer compression (extension) in the AF-BZGNR/h-BN(0001) heterostructure upon the changes in the width of the band gap for the $k=\pi$ Dirac point.

Analysis of Fig. 10b allows us to note the following regularities in the changes of the band gap width for the $k=\pi$ Dirac point: first, in case of bilayer compression on h-BN(0001) substrate the E_g band width for both electron subsystems (spin-up, spin-down) decreases to zero at $d=0.237$ nm; second, in equilibrium state of the atomic structure ($d=0.327$ nm) E_g is identical for both electron subsystems; third, in case of uniaxial extension of ZGNR E_g increases for both electron subsystems.

We should note that the influence of E_{ext} on PDOS of edge atoms of carbon, boron and nitrogen in the AF-BZGNR/h-BN(0001) heterostructure, while being identical to a certain extent, has considerable distinctions as illustrated in Fig. 11. For edge carbon atoms the size of sharp PDOS peaks shift in the proximity of the Fermi level depends on the strength of E_{ext} for the spin-up and spin-down electron configurations. In the absence of E_{ext} the shift of localized edge states in the proximity of the Fermi level is 0.43 eV (Fig. 11a). With the increase of field strength the said shift decreases 1.4 times at critical E_{ext} values (Fig. 11d). At the same time local magnetic moments of the edge carbon atoms in BZGNR decrease by 10% for both C1 and C2 atoms (see Fig. 8b). The response of edge magnetism to E_{ext} in the AF-BZGNR/h-BN(0001)

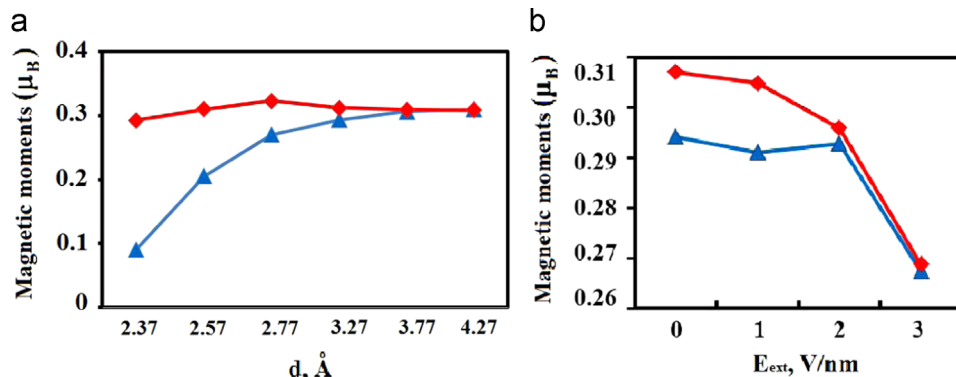


Fig. 8. (Color online) Magnetic moments of edge carbon atoms in the BZGNR/h-BN(0001) system depending on (a) the d distance and (b) the value of applied E_{ext} (V/nm) (C1 – red, C2 – blue).

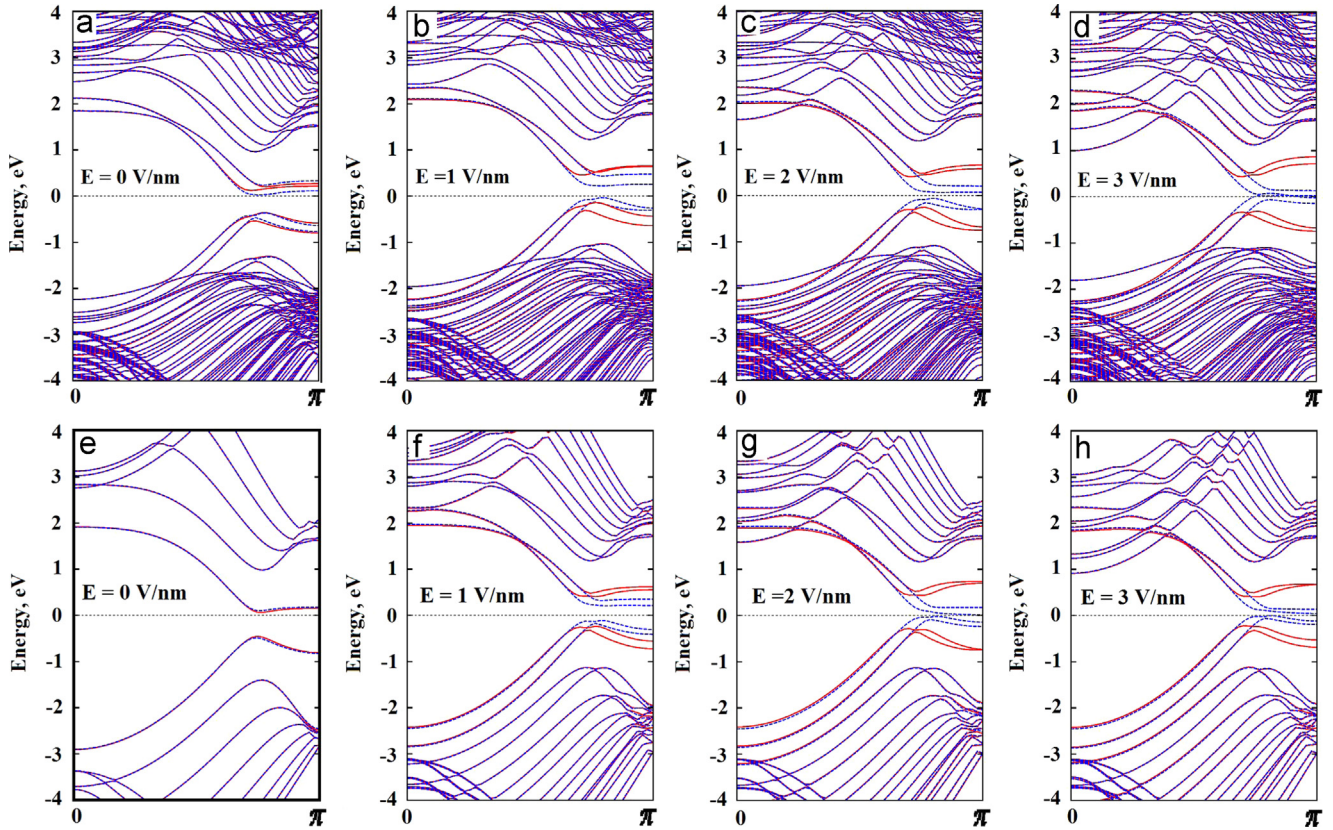


Fig. 9. (Color online) DFT-D2 spin-polarized calculation of the band spectrum (a–d) for the AF-BZGNR/h-BN(0001) heterostructure and (e–h) for suspended AF-BZGNR with various values of E_{ext} from left to right: red – spin-up, blue – spin-down.

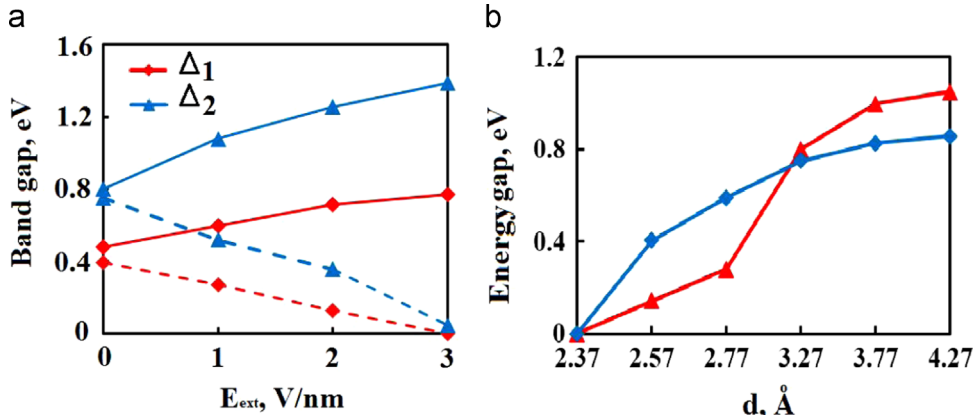


Fig. 10. (Color online) Variations of band gaps of the AF-BZGNR/h-BN(0001) interface depending on (a) E_{ext} (V/nm) with various spins configuration (solid line – spin-up, dashed line – spin-down) and (b) interplanar distance in the bilayer in $k = \pi$ Dirac point (red line – spin-up, blue line – spin-down).

heterostructure can be caused by partial suppression of spin exchange interaction at the nanoribbon edges by increasing E_{ext} .

Fig. 11a contains PDOS of boron (nitrogen) atoms in the first B1 (N1), second B2(N2) and third B3(N3) layers of the substrate. In the absence of E_{ext} the band structure of PDOS of substrate boron and nitrogen atoms contains $E_g=4.3$ eV energy gap and describes the crystalline state of h-BN. Occupied PDOS electron states below the Fermi level contain mostly contributions of $2p_z$ electrons of nitrogen atoms. Unoccupied PDOS of h-BN contain mostly contributions of $2p_z$ electrons of boron atoms – and are located above the Fermi level. The effect of E_{ext} for these crystalline states is manifested in stronger interaction of $2p_z$ -orbitals of carbon, boron and nitrogen. PDOS of two edge carbon atoms 1 and 2 in AF-BZGNR shown in Fig. 11b characterize the electron spectrum for the spin-up and spin-down

electron subsystems in case when the effect of interaction of the substrate is cancelled.

Analysis of Fig. 8b allows us to conclude that the induced local magnetic moment of the edge carbon atoms decreases in the presence of E_{ext} with the field increase. However, the heterostructure in question is magnetic. Remarkably, the effect of preserved local magnetic moment ($0.29\mu_B$) is observed on carbon atom C1 when low E_{ext} ranging from 0 V/nm to 2 V/nm is applied to the AF-BZGNR/h-BN (0001) semiconductor heterostructure. The nature of the effect causing stability of magnetic properties is unclear. The effect may be associated with the domination of exchange splitting in the edge states of carbon atoms (according to the Stoner model [37]) over the tendency of valence band and conduction band contraction [4]. We can also note that the presence of dielectric substrate will amplify the

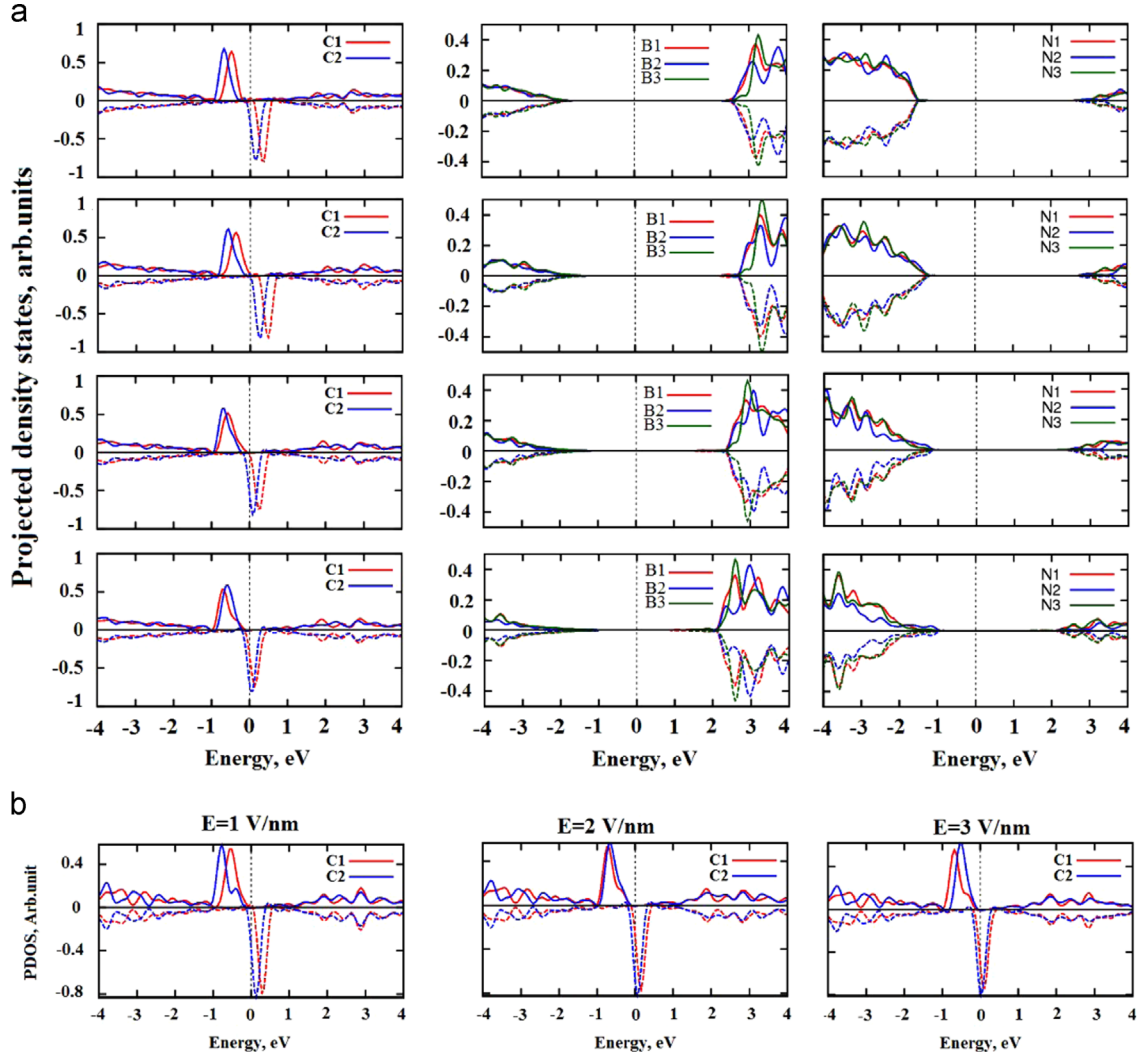


Fig. 11. (Color online) (a) PDOS of $2p_z$ -orbitals in C, B, and N atoms for both spins in the AF-BZGNR/h-BN(0001) heterostructure at the $E_{ext}=0; 1; 2; 3$ (top to down) and (b) PDOS of $2p_z$ -orbitals of edge C atoms in the AF-BZGNR at the $E_{ext}=1; 2; 3$ (left to right), where solid line – spin-up, dashed line – spin-down.

effect. The existence of the above-mentioned range of E_{ext} values should be attributed to the modulation of electron energy owing to dielectric screening of electron-electron interaction in AF-BZGNR/h-BN(0001) [38].

4. Conclusion

Thus, we used first-principles calculations based on the DFT to study the band spectrum and magnetic properties of a 1D graphene channel on h-BN functioning as a part of the AF-BZGNR/h-BN(0001) magnetic semiconductor heterostructure, in relation to three effects: uniaxial interlayer compression, E_{ext} and interaction with the substrate. We established critical values of uniaxial nanomechanical compression and E_{ext} for the AF-BZGNR/h-BN(0001) heterostructure providing for semiconductor–halfmetal–metal transitions for one of the spin electron configurations. As an important note, uniaxial interlayer compression and E_{ext} do not disrupt the magnetism of 1D graphene channel in the AF-BZGNR/h-BN(0001) heterostructure. Thus, we should speak about the magnetic semiconductor heterostructure of AF-BZGNR/h-BN(0001). The study has shown that magnetic properties of the AF-BZGNR/h-BN(0001) semiconductor heterostructure can be successfully varied in a wide range using their regulation with uniaxial interlayer compression and E_{ext} .

References

- [1] Y. Guo, W. Guo, C. Chen, J. Phys. Chem. 114 (2010) 13098.
- [2] Q. Tang, Z. Zhou, Z. Chen, Nanoscale 5 (2013) 4541.
- [3] Q. Tang, Z. Zhou, Mater. Prog. Mater. Sci. 58 (2013) 1244.
- [4] L.F. Huang, G.R. Zhang, Z.H. Zheng, P.L. Gong, T.F. Cao, Z. Zeng, J. Phys.: Condens. Matter 25 (2013) 055304.
- [5] F. Withers, T.H. Bointon, M. Dubois, S. Russo, M.F. Craciun, Nano Lett. 11 (2011) 3912.
- [6] R. Qin, et al., Phys. Rev. B 81 (2010) 233403.
- [7] V.V. Ilyasov, V.C. Nguyen, I.V. Ershov, D.C. Nguyen, J. Struct. Chem. 55 (2014) 209.
- [8] Y.W. Son, M.L. Cohen, S.G. Louie, Nature 444 (2006) 347.
- [9] V.V. Ilyasov, D.C. Meshi, V.C. Nguyen, I.V. Ershov, D.C. Nguyen, AIP Adv. 3 (2013) 092105.
- [10] V.V. Ilyasov, B.C. Meshi, V.C. Nguyen, D.C. Nguyen, Vestnik DSTU 7–8 (75) (2013) 75 (In Russian).
- [11] G. Giovanetti, et al., J. Phys. Pev. B: Cond. Matter 76 (2007) 073103.
- [12] V.V. Ilyasov, D.C. Meshi, V.C. Nguyen, I.V. Ershov, D.C. Nguyen, J. Appl. Phys. 115 (2014) 053708.
- [13] S. Dutta, A.K. Manna, S.K. Pati, Phys. Rev. Lett. 102 (2009) 096601.
- [14] J.B. Oostinga, H.B. Heersche, X. Liu, A.F. Maraud, L.M.K. Vandersypen, Nat. Mater. 7 (2008) 151.
- [15] A. Mattausch, O. Pankratov, Phys. Rev. Lett. 99 (2007) 076802.
- [16] Z. Zhang, C. Chen, X.C. Zeng, W. Guo, Phys. Rev. B 81 (2010) 155428.
- [17] T.S. Li, et al., Eur. Phys. J. B 64 (2008) 73.
- [18] G. Kim, S.H. Jhi, Appl. Phys. Lett. 97 (2010) 263114.
- [19] W.J. Yu, X. Duan, Sci. Rep. 3 (2013) 1248.
- [20] Z. Fang, J. Ni, J. Appl. Phys. 107 (2010) 104301.
- [21] Y.F. Guo, W.L. Guo, C.F. Chen, Phys. Rev. B 80 (2009) 085425.
- [22] Y.F. Guo, W.L. Guo, C.F. Chen, Appl. Phys. Lett. B 92 (2008) 243101.
- [23] Y. Zhang, X.L. Lu, E. Jiang, B. Teng, J.Q. Lu, J. Comput. Theoret. Nanosci. 8 (2011) 2448.

- [24] E.W. Castro, N.M.R. Peres, J.M.B. Lopes dos Santos, *J. Optoelectron. Adv. Mater.* 10 (2008) 1716.
- [25] B. Sahu, H. Min, A.H. MacDonald, S.K. Banerjee, *Phys. Rev. B* 78 (2008) 045404.
- [26] M.P. Lima, A. Fazzio, A.J.R. Silva, *Phys. Rev. B* 79 (2009) 153401.
- [27] H. Santos, A. Ayuela, L. Chico, E. Artacho, *Phys. Rev. B* 85 (2012) 245430.
- [28] V.V. Ilyasov, V.C. Nguyen, I.V. Ershov, in: Proceeding of the International meeting Ordering in Minerals and Alloys, Tuapse, Russia, 12–17 September 2013 (In Russian).
- [29] P. Giannozzi, et al., *J. Phys.: Cond. Matter* 21 (2009) 395502.
- [30] P. Hohenberg, W. Kohn, *Phys. Rev. B* 136 (1964) 864.
- [31] W. Kohn, L.J. Sham, *Phys. Rev. A* 140 (1965) 1133.
- [32] A.D. Corso, A. Pasquarello, A. Baldereschi, *Phys. Rev. B* 56 (R11) (1997) 369.
- [33] K. Burke, J.P. Perdew, M. Ernzerhof, *Int. J. Quantum Chem.* 61 (1997) 287.
- [34] S. Grimme, *J. Comput. Chem.* 25 (12) (2004) 1463.
- [35] C.W. Chen, M.H. Lee, S.J. Clark, *Nanotechnology* 15 (2004) 1837.
- [36] N.F. Mott, *Rev. Mod. Phys.* 40 (1968) 677.
- [37] E.G. Stoner, *Proc. R. Soc.* 165 (1938) 372.
- [38] X. Jiang, et al., *Appl. Phys. Lett.* 103 (2013) 133107.